Int. J. Solids Structures Vol. 16, pp. 515–536

0020-7683/80/0601-0515/$02.00/0

STRAIN RATE AND STRAIN RATE HISTORY EFFECTS ON THE DYNAMIC BEHAVIOR OF METALLIC MATERIALS

HAN C. WU† and M. C. YIP‡
Division of Materials Engineering, University of Iowa, Iowa City, IA 52242, U.S.A.

(*Received* 17 *January* 1979; *in revised form* 30 *August* 1979)

Abstract—The constitutive equations for strain hardening (f.c.c. metals and alloys) and strain softening-hardening metallic materials (b.c.c. metals and alloys) have been developed. The development is within the framework of the endochronic theory of viscoplasticity. In this discussion, the intrinsic time is dependent on the plastic strain rate.

The strain rate and the strain rate history effects have been investigated. Sets of constant-strain-rate stress–strain curves have been theoretically obtained for both classes of metallic materials mentioned. The strain rate history effect is studied in terms of low–high and high–low strain rate change test sequences. For a fixed strain rate history in the case of strain hardening materials, a similar pattern of subsequent material behavior is obtained, independent of the strain magnitude at which the strain rate change takes place. However, in the case of strain softening–hardening materials, the strain magnitude at which the strain rate change occurs affects the subsequent material behavior.

Theoretical results are compared with experimental data found in the literature.

1. INTRODUCTION

The study of dynamic plasticity of metallic materials has become increasingly important in recent years. It is now clear that many practical problems such as brittle fracture, stress wave propagation and high rate forming can only be satisfactorily treated if the rate dependence of the plastic behavior of the material is taken into account. The behavior of materials under dynamic loads is obviously of considerable interest in most mechanical analyses of design problems where dynamic loads are present. Unfortunately, much of the engineering design today is still based on the static properties of the material rather than dynamic properties. Further understanding of the dynamic properties would lead to improvement in engineering design.

Dynamic plasticity of metallic materials was first seriously investigated in 1872 by Hopkinson[1]. In this paper, the rupture of iron wire by impact loading was discussed. In the last 30 yr, a large volume of papers, such as Bell[2], Ripperger[3], Malvern[4], Lindholm[5] and Campbell and Marsh[6], to name only a few, have presented the results of impact or impulsive loading of a bar. Stress wave propagation in plate and cylinder, and propagation of cracks using high speed testing machines have also been investigated, all with the purpose of defining the intrinsic dynamic mechanical properties of the materials.

The influence of strain rate on the mechanical response has been studied extensively in the past. But in most experiments, whether they involved tension, compression or torsion, the strain rate was held constant. This situation was particularly true in a high strain rate testing where changes of strain rate were difficult to obtain. Unfortunately, constitutive relations derived on the basis of experiments at single strain rates are, in a sense, oversimplification.

A strain rate history independent (but strain rate dependent) theory was presented by Sokolovsky[7] and Malvern[8]. The theory assumes that the plastic strain rate is a function of the overstress, which implies that the current stress depends only on the current strain rate but not on the past strain rate. The overstress is the amount of stress by which the applied stress exceeds the corresponding flow stress for the same strain at vanishingly small strain rate. Unfortunately, the foregoing assumption does not agree with the more recent experiments which show that the current stress depends on the history of strain rate. However, the nature of strain rate history dependence is not well understood at the present time.

†Associate Professor.
‡Graduate Assistant. Present address the Department of Power Mech. Engng., National Tsing Hua University, Hsinchu, Taiwan.

The strain rate history effect was first investigated by Campbell and Duby[9] in 1956. In this study, the static reloading in compression of dynamically prestrained specimen of mild steel was investigated. It was found that the stress required to produce a given amount of plastic strain was less for the specimen prestrained dynamically than for those prestrained statically. In 1961, Smith[10] presented test results of dynamic stress–strain behavior of low-carbon steel subjected to a change in strain rate from 2.22×10^{-7} per sec to 7.5 per sec and also those from a high strain rate to a low strain rate loading sequence. Also in 1971, Nicholas[11] presented test results to show the strain rate history effect of 1020 steel with a change of shear strain rate from 10^{-4} per sec to 25 per sec. Results from these papers showed that strain rate history effect was very pronounced in steel. Qualitative differences were found among experimental results of Smith's and Nicholas' studies. No explanations to this effect have been given, however, in the literature. In the present paper, a unified approach will be given which shows that these seemingly incompatible observations are truly the anticipated material response under different loading conditions. All the experiments mentioned above were conducted on steel. No data was found available for other body-centered-cubic (b.c.c.) metallic materials.

The strain rate history effect of face-centered-cubic (f.c.c.) polycrystalline metallic materials was discussed in a number of papers. Lindholm[12] examined the effect of previous strain rate history on the stress–strain curve of annealed high purity aluminum by alternately strain cycling the same specimen at widely divergent strain rates. In 1968, Klepaczko[13] studied strain rate history effect of polycrystalline aluminum (99.8% Al) and presented strain hardening curves obtained from shear tests at room temperature with a change in strain rate from 1.66×10^{-5} per sec to 0.624 per sec. Results of a reversed test sequence for the same strain rates were also presented. In 1972, Frantz and Duffy[14] presented curves showing the dynamic stress–strain behavior in shear of 1100-0 aluminum subjected to a sharp increase in strain rate from 10^{-5} per sec to 8.5×10^{2} per sec imposed at several strain magnitudes in the range of 0.01–0.15. Klepaczko[15] investigated the strain rate and strain rate history behavior of copper (98.5% Cu) under tensile and also torsional load with a strain rate ranging between 2.2×10^{-3} per sec and 6.1×10^{-1} per sec in tensile testing and up to 9×10^{2} per sec in torsional testing. In 1977, Klepaczko, Frantz and Duffy[16] presented the additional results of copper and lead showing that the materials are affected by the strain rate history. Additional data of strain rate history effect have also been reported for two kinds of aluminum alloy by Nicholas[11] in 1971. The results of above papers show that the strain rate history effect of f.c.c. and b.c.c. metallic materials are different. The difference will be discussed and explained in this paper from the viewpoint of the proposed theory.

The above review indicates that the strain rate history effects are very important in both b.c.c. and f.c.c. metallic materials. A more general analysis of strain rate history effect is needed. Unfortunately, most of the papers reviewed above dealt only with experimental data and testing procedures. The theoretical work based on continuum mechanics has not progressed beyond the strain rate effect on f.c.c. metals. Theoretical predictions in strain rate effect of b.c.c. metallic materials and strain rate history effect of both b.c.c. and f.c.c. metallic materials cannot be found. Thus a unified analysis of both of these factors is a much needed effort and constitutes the main purpose of this paper.

The proposed theoretical analysis is based on the endochronic theory of plasticity developed by Valanis[17, 18]. This theory is a phenomenological theory that conforms with thermodynamics and continuum mechanics. It is not the purpose of this paper to discuss the physical foundation of the theory. However, the equations to be discussed are useful in the engineering analysis and design.

A brief summary of the updated version of the endochronic theory is given in Section 2. Within the framework of this theory, the constitutive equation for strain hardening materials (f.c.c. metals and alloys) has been developed for the one dimensional dynamic response and is presented in Section 3. In this development, the intrinsic time is proposed to depend on a function of strain rate. In Section 4, the theory is applied to provide theoretical predictions in the mechanical behavior of strain softening–hardening materials (b.c.c. metallic materials) under dynamic loadings. Generally, the behavior of this class of material is quite different than that of f.c.c. metals and alloys. The difference is accounted for by the functional relationship between the intrinsic time z and the intrinsic time measure ζ. This relationship is thoroughly

investigated in the paper. The constitutive equations are also applied to investigate the strain rate history effect for both the b.c.c. and f.c.c. metallic materials. The theoretical results are then compared with experimental data reported in the literature.

2. BRIEF SUMMARY OF ENDOCHRONIC THEORY OF PLASTICITY

The endochronic theory of viscoplasticity developed by Valanis[17] is based on the notion of intrinsic time and the thermodynamic theory of internal variables. Since most of the materials are, in general, strain history dependent, a time measure $d\zeta$ is defined such that

$$d\zeta^2 = P_{ijkl}\, d\epsilon_{ij}\, d\epsilon_{kl} \tag{1}$$

where ϵ_{ij} is the strain tensor and P_{ijkl} is a positive definite material tensor, which for isotropic materials take the form

$$P_{ijkl} = p_1\delta_{ij}\delta_{kl} + p_2\delta_{ik}\delta_{jl}. \tag{2}$$

In eqn (2) p_1 and p_2 are material constants satisfying $p_1 + p_2/3 \geq 0$ and $p_2 \geq 0$. In addition, a time scale $z(\zeta)$ is introduced such that $dz/d\zeta > 0$.

This concept together with the thermodynamic theory of the internal variables gives the following explicit constitutive equation for isotropic materials under small isothermal deformation:

$$\sigma_{ij} = \delta_{ij}\int_0^z \lambda(z-z')\frac{\partial \epsilon_{kk}}{\partial z'}\,dz' + 2\int_0^z \mu(z-z')\frac{\partial e_{ij}}{\partial z'}\,dz' \tag{3}$$

where σ_{ij} is the stress tensor, e_{ij} is the deviatoric part of ϵ_{ij}; δ_{ij} is the Kronecker's delta; and $\lambda(z)$ and $\mu(z)$ are heredity functions. But the definition of intrinsic time in eqn (1) has led to difficulties in cases where the history of deformation involves unloading. Valanis[18] has since introduced a new concept of intrinsic time to overcome these difficulties. In the one dimensional case the new intrinsic time ζ is defined as

$$d\zeta = \left|d\epsilon - k_1\frac{d\sigma}{E_0}\right| \tag{4}$$

where k_1 is a positive scalar such that $0 \leq k_1 \leq 1$ and E_0 is the elastic modulus. Generalizing to three dimensions and r internal variables, a strain like tensor θ_{ij} is defined as

$$\theta_{ij} = \epsilon_{ij} - \phi_{ijkl}\sigma_{kl} \tag{5}$$

and

$$Q_{ij} = e_{ij} - \frac{k_1}{2\mu_0}s_{ij} \tag{6}$$

where ϕ_{ijkl} is a positive definite symmetric fourth-order tensor; Q_{ij} is the deviatoric part of θ_{ij}; μ_0 is the shear modulus; and s_{ij} is the deviatoric part of σ_{ij}. Based on the formulation in Ref.[17], the response of metals in the small deformation region with an elastic hydrostatic response can be written as

$$\sigma_{kk} = 3K\epsilon_{kk} \tag{7}$$

and

$$s_{ij} = 2\int_0^z \mu(z-z')\frac{\partial e_{ij}}{\partial z'}\,dz' \tag{8}$$

where K is the bulk modulus. If the function $\mu(z)$ is defined as

$$\mu(z) = \mu_0 G(z) \tag{9}$$

where $G(0) = 1$, and using the Laplace Transformation technique, eqn (8) together with eqns (6) and (9) can be written as

$$s_{ij} = 2\mu_0 \int_0^z \rho(z - z') \frac{dQ_{ij}}{dz'} dz' \tag{10}$$

where $\rho(z)$ is related to $G(z)$ by the integral equation

$$\rho(z) - k_1 \int_0^z \rho(z - z') \frac{dG}{dz'} dz' = G(z). \tag{11}$$

The solution of this integral equation in the case of two internal variables is obtained by the Laplace transform technique under the assumption of k_1 approaching to 1. The result is

$$E_0 \rho(z) = \frac{E_0}{1 - k_1} e^{-(\alpha_0/1-k_1)z} + E_1 e^{-\alpha z} + E_2 \tag{12}$$

where α_0, α, E_1 and E_2 are material parameters. In the case of uniaxial stress, the constitutive equation is given by

$$\sigma = E_0 \int_0^z \rho(z - z') \frac{d\theta}{dz'} dz' \tag{13}$$

where $\theta = \epsilon - (\sigma/E_0)$ for $k_1 \to 1$ is the plastic strain, and eqn (4) can be written as

$$d\zeta = |d\theta| \tag{14}$$

3. STRAIN HARDENING MATERIALS

In this section, the endochronic theory with the new definition of intrinsic time, which has been briefly summarized in the previous section, is applied to obtain the stress–strain relation for strain hardening materials subject to strain rate and its history effects.† The strain hardening behavior is a characteristic of most f.c.c. metallic materials.

The definition of intrinsic time by Valanis[18] is not readily applicable to describe the strain rate and strain rate history dependence of this class of material. A modified form is thus proposed which makes the constitutive equation depend not only on the deformation but also on the strain rate and strain rate history. The theoretical stress–strain relations for various constant strain rates (in the range of 10^{-4}–10^3 per sec) are then presented and the results compared with the experimental data of Karnes and Ripperger[19] for annealed aluminum. Based on this constitutive equation, the loading–unloading–reloading loop is discussed and comparison with the experimental data of Papirno and Gerard[20] for aluminum is presented. Also, the strain rate history effect is thoroughly investigated and results compared with the experimental data of Frantz and Duffy[14] for 1100-0 aluminum.

In the case of uniaxial stress, the constitutive equation by use of the new intrinsic time was obtained by Valanis[18] and was mentioned in eqn (13). However, the dynamic effect was not considered during the derivation of this equation in [18]. To accomodate the dynamic response of metallic materials, the new intrinsic time measure is modified. A more general form of the intrinsic time measure involving strain rate effect can be written as

$$d\zeta = k(\dot{\theta})|d\theta|. \tag{15}$$

†While the equations in Section 2 are generally valid, the discussion of the strain rate and the strain rate history effects presented herein is restricted to the one-dimensional case.

It is shown in the Appendix that the above definition of intrinsic time conforms that originally given by Valanis[18].

In this case, eqn (13) is written as

$$\sigma = E_0 \int_0^z \rho(z - z') \frac{1}{k(\dot{\theta})} \frac{d\zeta'}{dz'} dz'. \tag{16}$$

Since $k(\dot{\theta})$ is a function of strain rate, then eqn (16) is a constitutive equation encompassing the strain rate and strain rate history effect. As k_1 approaches to 1, the function $\rho(z)$ shown in eqn (12) can be written as

$$E_0\rho(z) = E_0\rho_0\delta(z) + E_0\rho_1(z) \tag{17}$$

where ρ_0 is a constant, $\delta(z)$ is delta function and $\rho_1(z)$ is given by

$$E_0\rho_1(z) = E_1 e^{-\alpha z} + E_2. \tag{18}$$†

Then, from eqn (16), it follows that

$$\sigma = E_0\rho_0 \frac{1}{k(\dot{\theta})} \frac{d\zeta}{dz} + E_0 \int_0^z \rho_1(z - z') \frac{1}{k(\dot{\theta})} \frac{d\zeta'}{dz'} dz'. \tag{19}$$

At $z = 0$, eqn (19) reduces to

$$\sigma = E_0\rho_0 \frac{1}{k(\dot{\theta})} \frac{d\zeta}{dz}\bigg|_{z=0}. \tag{20}$$

It is seen that $d\zeta/dz$ is indeterminate when $z = 0$. However, when $z > 0$ the derivative $d\zeta/dz$ exists, and specifically at $z = 0_+$ the limit of $d\zeta/dz$ can be obtained. In fact, the point 0_+ is the point of deviation from the elastic response. At this point, the stress must be equal to the yield stress, and eqn (20) becomes

$$|\sigma|^2 = E_0^2\,\rho_0^2 \left[\frac{1}{k(\dot{\theta})}\right]^2 \left(\frac{d\zeta}{dz}\right)^2\bigg|_{z=0_+} \overset{\text{def.}}{=} \sigma_y^2. \tag{21}$$

Therefore, the yield stress σ_y defined in eqn (21) is not a constant but is a function of strain rate due to the presence of the strain rate sensitivity function $k(\dot{\theta})$.

3.1 *Loading curves with constant strain rate*

In a loading process, the increment of plastic strain is positive. Then, eqn (15) becomes

$$d\zeta = k(\dot{\theta})\, d\theta \tag{22}$$

where $k(\dot{\theta})$ is constant for a constant strain rate. Moreover, if the following relation is used

$$z = \frac{1}{\beta}\log(1 + \beta\zeta) \tag{23}$$

where β is a material parameter, then from the constitutive equation (16) and the associated relations, it is possible to establish under the condition of constant strain rate, that

$$\sigma = \frac{E_0(1+\beta\zeta)}{\beta_1(n_0 - k_1)}\{1 - (1+\beta\zeta)^{-(n_0 - k_1/1 - k_1)}\} + \frac{E_1(1+\beta\zeta)}{\beta_1 n}\{1 - (1+\beta\zeta)^{-n}\} + \frac{E_2\zeta}{k} \tag{24}$$

†Because of the complexity of the constitutive equation and the fact that the number of material parameters increases with the number of internal variables, it is natural to strive for the minimum number of internal variables which will suffice in the accurate and acceptable prediction of the material response. Two internal variables are used throughout this work.

where

$$n = \frac{\alpha}{\beta} + 1 \tag{25}$$

$$n_0 = \frac{\alpha_0}{\beta} + 1 \tag{26}$$

and

$$\beta_1 = \beta k. \tag{27}$$

At the initial point of the intrinsic time measure $\zeta = 0_+$ (i.e. when θ is equal to zero), σ is equal to the yield stress. Hence,

$$\sigma_y = \frac{E_0}{\beta_1(n_0 - k_1)}. \tag{28}$$

For large ζ (or θ), eqn (24) approaches to an asymptotic line given by

$$\sigma = \sigma_y(1 + \beta_1\theta) + \frac{E_1}{\beta_1 n}(1 + \beta_1\theta) + E_2\theta. \tag{29}$$

Defining σ_0 as the intercept of this asymptotic line with the stress axis, E_t, the tangent modulus of the asymptotic line and E_p, the initial slope of the stress-plastic strain curve, it is easy to establish that

$$\frac{E_1}{\beta_1 n} = \sigma_0 - \sigma_y \tag{30}$$

$$\beta_1 = \frac{E_t - E_2}{\sigma_0} \tag{31}$$

and

$$\frac{E_0}{1 - k_1} + E_1 + E_2 = E_p \tag{32}$$

where σ_0 and σ_y are functions of strain rate. Thus, for each strain rate, there corresponds a stress-plastic strain curve. The experimental data of Karnes and Ripperger[19] for annealed aluminum show that the stress-plastic strain relations at different strain rates are almost parallel to each other at least in the range of $\theta < 2\%$; i.e. E_t remains constant for all strain rates.† Based on these experimental curves and eqn (31), and assuming k to be equal to 1 on the curve of reference strain rate, Fig. 1 has been constructed and the data points are nicely fitted by the following expression for the strain rate range from 10^{-4} to 10^3 s^{-1}

$$k(\dot{\theta}) = 1 - k_s \log\left(\frac{\dot{\theta}}{\dot{\theta}_0}\right) \tag{33}$$

†For the nonparallel case reported by Hauser *et al.*[22], this theory is still valid with the modification that E_t depend on the strain rate. In this case E_0 should also depend on strain rate for the theory to be self consistent. It can be shown from eqns (28), (30) and (31) that

$$E_0 = (n_0 - k_1)\left(E_t - E_2 - \frac{E_1}{n}\right).$$

It is seen that E_0 increases with E_t, but the change in E_0 is too small to show in the graph.

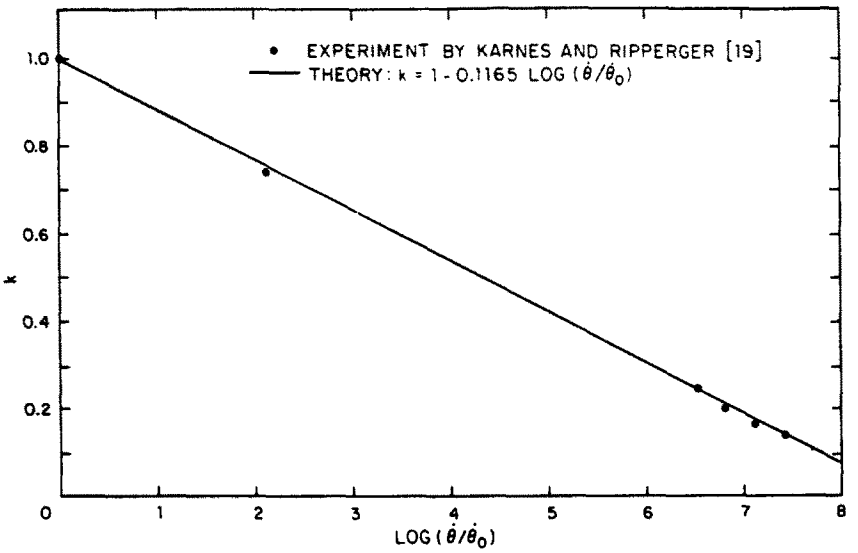

Fig. 1. The strain rate sensitivity function for annealed aluminum.

where k, is a material parameter; and $\dot{\theta}_0$ is a reference strain rate† taken as 1.5×10^{-4} per sec in this case. This expression has the same form as that of Lin and Wu[21]. The only difference is that in eqn (33) the plastic strain rate is used instead of the total strain rate. In fact, the plastic strain rate is approximately equal to the total strain rate in the large strain range. Only in the small strain range is the difference significant. However, in this range the strain rate is difficult to monitor experimentally and the results are less reliable.

The material constants, E_t, σ_0, σ_y can be measured directly from each constant strain rate stress–strain curve. Theoretically, eqn (28), (30), (31) and (32) are not sufficient for the determination of the five parameters, i.e. β_1, n_0, n, E_1 and E_2. Thus, the constitutive equation may be rewritten in the following more convenient form:

$$\sigma = (1+\beta_1\theta)[\sigma_0 - (\sigma_0 - \sigma_y)(1+\beta_1\theta)^{-n}] + E_2\theta \tag{34}$$

in which β_1, n, and E_2 are parameters yet to be determined. Equation (34) has been obtained from eqns (24), (28), (30), (31) and (33).

The parameters β_1, n and E_2 are determined by the trial and error method so that the theoretical curve agrees with the experimental reference curve. Note that β_1 is related to E_2 by eqn (31), so that only n and E_2 can be varied.

Equation (34) describes a set of stress–strain curves at various constant strain rates. The theoretical results and the experimental data of high purity aluminum at the strain rates from 1.5×10^{-4} per sec to 5000 per sec[19] are shown in Fig. 2. The comparison is satisfactory for the set of stress–strain curves. The parameters of this material are determined to be

$$E_0 = 10 \times 10^6 \text{ psi } (6.89 \times 10^4 \text{ MPa}) \quad \beta = 180$$
$$\sigma_0^0 = 1 \times 10^3 \text{ psi } (6.89 \text{ MPa}) \quad n = 25$$
$$\sigma_y^0 = 0.75 \times 10^3 \text{ psi } (5.17 \text{ MPa}) \quad E_2 = 0$$

where σ_0^0 and σ_y^0 are the intercept of the asymptotic line with the stress axis and the initial yield stress for the reference stress–strain curve. $\dot{\theta}_0$ is assumed to be 1.5×10^{-4} per sec in this investigation. The strain rate sensitivity function k has already been determined in Fig. 1.

†Equation (31) determines the empirical relation $\beta_1 = \beta_a - \beta_b \log(\dot{\theta}/\dot{\theta}_0)$, where β_a and β_b are material parameters. The reference strain rate $\dot{\theta}_0$ is a convenient strain rate within the range of validity of eqn (33). By choosing a different $\dot{\theta}_0$ the β_1 vs $\log(\dot{\theta}/\dot{\theta}_0)$ relation is just shifted along the $\dot{\theta}$ axis and the parameter β_a needs to be adjusted accordingly. Equation (33) is the normalized form of the above equation with respect to the material constant β. It is a reasonable approximation to take $\dot{\theta}_0 = 1.5 \times 10^{-4}\,s^{-1}$ as the "quasi-static" strain rate. At this strain rate, it is convenient to put $k = 1$ and $\beta_a = \beta$.

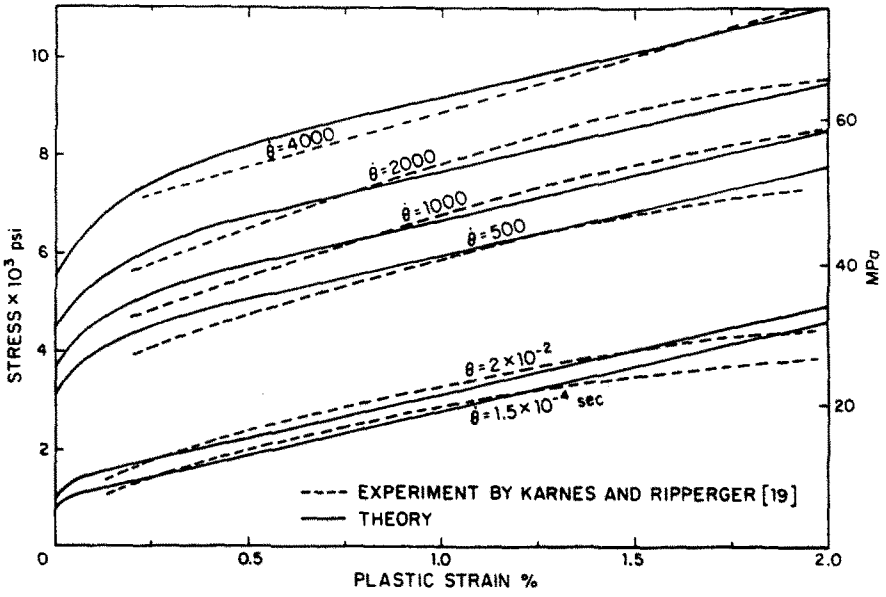

Fig. 2. Constant strain rate stress–strain curves for annealed aluminum.

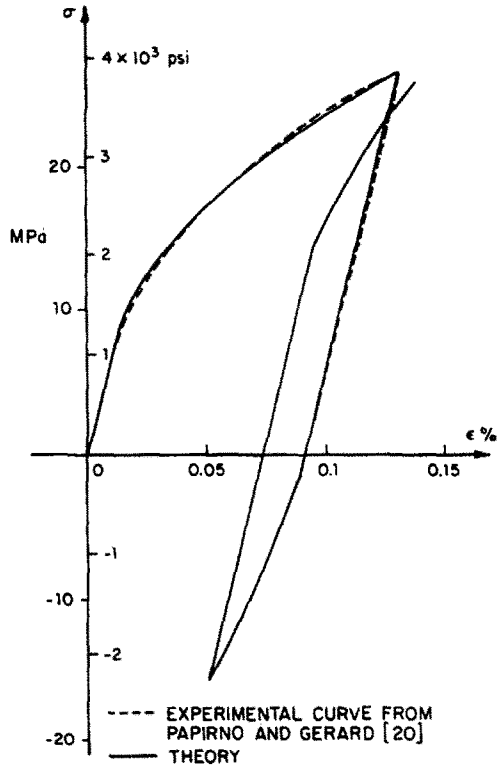

Fig. 3. Hysteresis loop for pure aluminum.

3.2 *Hysteresis loops*

Equations for loading–unloading–reloading processes at constant strain rate can be obtained in closed forms by the integration of eqn (16). Appropriate forms of eqns (15) need to be used in this exercise. It suffices to mention only that a drop in stress of magnitude $2\sigma_y(1+\beta\zeta^*)$ occurs during the elastic part of the unloading process, where unloading starts at ζ^*. Similarly, a rise in stress of $2\sigma_y(1+\beta\zeta^{**})$ occurs during the elastic part of the reloading process. The process of reloading is assumed to begin at ζ^{**}. Figure 3 illustrates a theoretical hysteresis loop. Experimental curve obtained by Papirno and Gerard[20] is also shown for comparison. The material in consideration is that of the commercially pure aluminum. The material parameters

have been determined as

$$E_0 = 10 \times 10^6 \text{ psi } (6.89 \times 10^4 \text{ MPa}) \quad \beta = 695$$
$$\sigma_0^0 = 2.35 \times 10^3 \text{ psi } (16.19 \text{ MPa}) \quad n = 10$$
$$\sigma_y^0 = 1.25 \times 10^3 \text{ psi } (8.61 \text{ MPa}) \quad E_2 = 0.$$

It is remarked that the subject of hysteresis loop was investigated by Valanis[18]. However, the strain rate and the strain hardening effects were not included in his presentation.

3.3 *Strain rate history effect in the constitutive equation*

The strain rate effect in the constitutive equation has been discussed in the previous subsections. It was shown that the stress–strain relationship for the strain rate sensitive materials may be described by a set of curves each corresponding to a specific strain rate. In this subsection, the effect of strain rate history in the constitutive equation is examined. In general, the discussion is separated into two parts. The first part is related to the strain rate changing from low to high during testing and the second part is that of a high–low strain rate change test sequence. These two parts are discussed in detail below.

(a) *Low–high strain rate change test sequence.* Since the function $k(\dot{\theta})$ is dependent on the strain rate, its value is not the same before and after the change in strain rate. If the strain rate change occurs at $\theta = \theta^*$ (or $\zeta = \zeta^*$), eqn (15) becomes

$$d\zeta = \begin{cases} k_l \, d\theta & \text{for } \zeta \le \zeta^* \\ k_h \, d\theta & \text{for } \zeta > \zeta^* \end{cases} \tag{35}$$

where k_l and k_h are the values of k corresponding to the low and high strain rates, respectively. The constitutive equation for the range of $\zeta \le \zeta^*$ is given in eqn (34) with $k = k_l$. For the range of $\zeta > \zeta^*$, the constitutive equation is given by

$$\sigma = E_0 \int_0^{z^*} \rho(z - z') \left(\frac{1}{k_l}\right) \frac{d\zeta'}{dz'} dz' + E_0 \int_{z^*}^{z} \rho(z - z') \left(\frac{1}{k_h}\right) \frac{d\zeta'}{dz'} dz'. \tag{36}$$

Integrating the above equation, one obtains

$$\sigma = \frac{\sigma_y^0}{k_h}(1 + \beta\zeta) + \frac{(\sigma_0^0 - \sigma_y^0)}{k_l}(1 + \beta\zeta)\left\{\left(\frac{1 + \beta\zeta^*}{1 + \beta\zeta}\right)^n - (1 + \beta\zeta)^{-n}\right\}$$
$$+ \frac{\sigma_0^0 - \sigma_y^0}{k_h}(1 + \beta\zeta)\left\{1 - \left(\frac{1 + \beta\zeta^*}{1 + \beta\zeta}\right)^n\right\} + \frac{E_2\zeta^*}{k_l} + \frac{E_2(\zeta - \zeta^*)}{k_h} \tag{37}$$

and

$$\theta = \theta^* + \frac{\zeta - \zeta^*}{k_h}. \tag{38}$$

The effect on the material behavior due to the strain rate history considered here is shown schematically in Fig. 4. The solid line is the loading curve with a change in strain rate from low to high at point M where the plastic strain is equal to θ^*. The dotted line PQ denotes the constant strain rate stress–strain curve at the previously described high strain rate. The stress at points M, P and N can be found and it is obvious that at the point of change in strain rate a jump in stress of magnitude

$$\left(\frac{1}{k_h} - \frac{1}{k_l}\right)\sigma_y^0(1 + \beta\zeta^*)$$

occurred. Since N does not coincide with P, the difference in stress is attributed to the strain rate history effect.

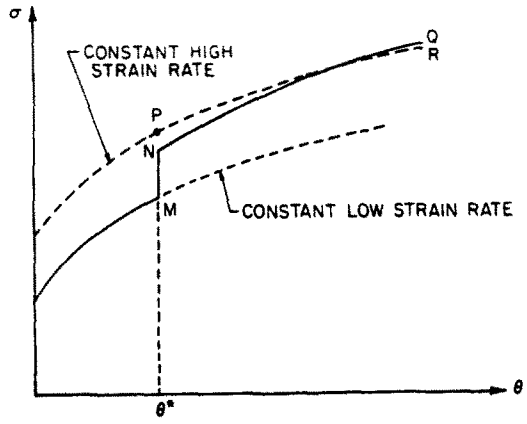

Fig. 4. Schematic presentation of response of strain hardening materials to low–high strain rate change test sequence.

Frantz and Duffy[14] presented experimental curves showing the dynamic stress–strain behavior in shear of 1100-0 aluminum subjected to a sharp increase in shear strain rate from 10^{-5} per sec to 8.5×10^2 per sec imposed at several levels of strain in the range of 0.01–0.15. Figure 5 shows the results of both theoretical calculations and experiment. The theoretical curves for low constant strain rate before the change of strain rate and for high constant strain rate are calculated by use of eqn (34) with $k_l = 1$ and $k_h = 0.75$, respectively. The other material parameters are determined as

$$\sigma_0^0 = 3 \times 10^3 \text{ psi } (20.67 \text{ MPa}) \qquad \beta = 5$$
$$\sigma_y^0 = 1.25 \times 10^3 \text{ psi } (8.61 \text{ MPa}) \qquad n = 30$$
$$E_2 = 35 \times 10^3 \text{ psi } (2.41 \times 10^2 \text{ MPa}).$$

In this figure, the theoretical results are in qualitative agreement with the experimental data

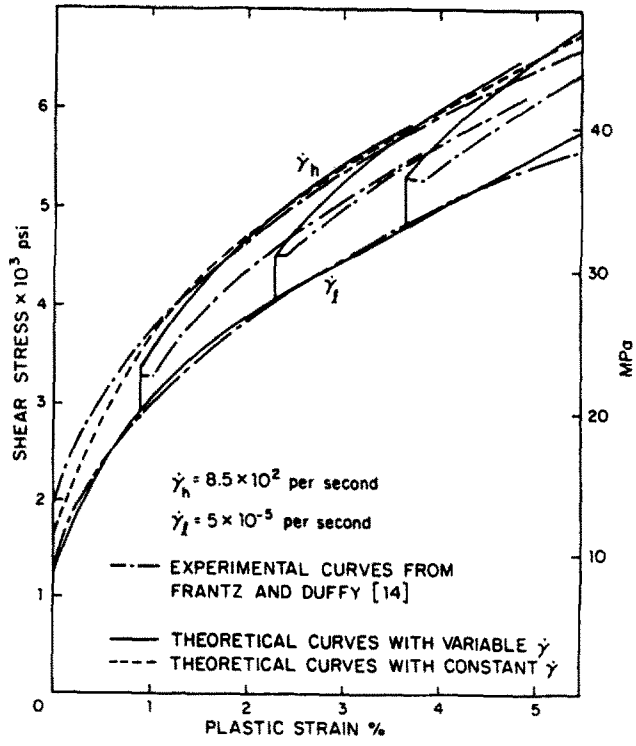

Fig. 5. Behavior of 1100-0 aluminum in shear under low–high strain rate change test sequence.

for strain rate change test sequence at several strain levels in the range up to 0.05. But the jumps in stress at the change of strain rate as predicted by the theory are slightly larger than those actually obtained by experiment. Also in experiments, after each jump, a drop in stress appeared which was not anticipated by the theory. However, in a different series of experiments by Senseny, Duffy and Hawley[23] on essentially the same material, the stress drop was not observed.

At large strain range, the stress calculated from eqn (37) rises above the curve of high constant strain rate. It can be shown that the stress at Q in Fig. 4 is greater than that at R by a constant amount $\sigma_0^0\beta\theta^*[(k_l/k_h)-1]$. This phenomenon is not experimentally observed. But in view of the fact that this difference in stress is small and the over-shooting occurs only at larger strain range (>3%), the theoretical results are considered to represent a reasonable first approximation for a small deformation theory.

(b) *High–low strain rate change test sequence.* In this sub-section, the sequence of strain rate change is reversed. The strain rate is first kept at a high rate and then changed into a lower rate. The solid line in Fig. 6 illustrates schematically this change; whereas the dotted lines represent the stress–strain curves at constant strain rates. Using a similar procedure as in the last sub-section, the constitutive equation for $\zeta > \zeta^*$ can be expressed as

$$\sigma = \frac{\sigma_y^0}{k_l}(1+\beta\zeta) + \frac{\sigma_0^0-\sigma_y^0}{k_h}(1+\beta\zeta)\left\{\left(\frac{1+\beta\zeta^*}{1+\beta\zeta}\right)^n - (1+\beta\zeta)^{-n}\right\} + \frac{\sigma_0^0-\sigma_y^0}{k_l}(1+\beta\zeta)\left\{1-\left(\frac{1+\beta\zeta^*}{1+\beta\zeta}\right)^n\right\} + \frac{E_2\zeta^*}{k_h} + \frac{E_2(\zeta-\zeta^*)}{k_l} \tag{39}$$

and

$$\theta = \frac{\theta^*}{k_h} + \frac{\zeta-\zeta^*}{k_l} \tag{40}$$

Again, in Fig. 6, a drop in stress of

$$\left(\frac{1}{k_h}-\frac{1}{k_l}\right)\sigma_y^0(1+\beta\zeta^*)$$

from point M to point N has been resulted. The stresses are different between N and P which indicates a strain rate history effect. Also, for the same large strain, the stress at Q is less than R by a constant value of $\sigma_0^0\beta\theta^*[1-(k_h/k_l)]$.

Klepaczko[13] presented experimental curves of copper subjected to a sudden decrease in strain rate from 0.624 per sec to 1.66×10^{-5} per sec at several strain levels in the range of

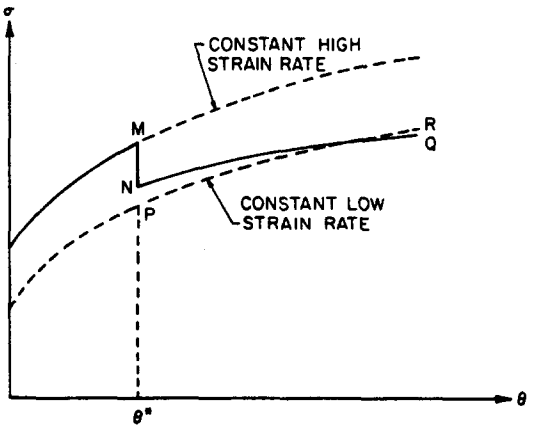

Fig. 6. Schematic presentation of response of strain hardening materials to high–low strain rate change test sequence.

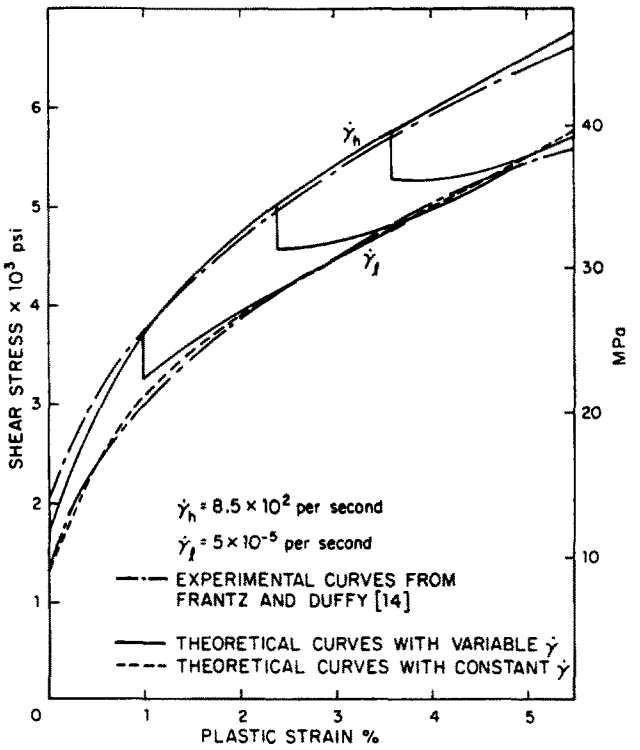

Fig. 7. Behavior of 1100-0 aluminum in shear under high–low strain rate change test sequence.

0.15–0.50. However, no data is provided in the strain range within 0.05. Figure 7 shows the theoretical curves obtained by use of the same parameters used in the construction of Fig. 5.

It should be remarked that the shape of the stress–strain curve after the strain-rate drop is dependent on the strain level where drop occurs. Theoretically, a critical strain level may be defined at which the slope of the stress strain curve is zero immediately after the strain rate drop. For the present example the critical strain is equal to 2.1%. It is seen from Fig. 7 that the stress–strain curves following the drop in strain rate at 2.4 and 3.6% strains are qualitatively different from that at 1% strain. Those for higher strain levels exhibit the same trend as those obtained experimentally by Klepaczko.

4. STRAIN SOFTENING–HARDENING MATERIALS

The strain softening–hardening behavior in the stress–strain curve is observed in some engineering materials typified by the curve shown in Fig. 8. In this curve, the stress rises with almost negligible plastic deformation to the upper yield point. At this point, the material begins to yield, with a simultaneous drop in stress required for continued deformation. Once defor-

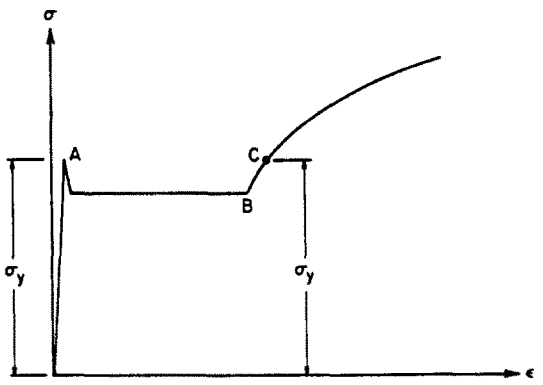

Fig. 8. A typical stress–strain curve of b.c.c. metallic materials.

mation has been initiated, it continues at constant stress until the entire body has been plastically deformed. An increase in stress is then required to continue the deformation process. This important effect occurs in iron and low-carbon steel which are body-centered-cubic (b.c.c.) metallic materials.

In this section, the dynamic behavior of this kind of material is described using the proposed theory. To achieve this, the relationship between ζ and z is first discussed. Explicit relations for ζ and z are given for hardening as well as softening materials. For strain softening–hardening materials, a critical value ζ_{cr} is introduced at which the behavior of materials changed from softening to hardening. Using this ζ–z relation, the constitutive equation for b.c.c. metals is obtained. The equation is then applied to investigate the strain-rate and strain rate history effects of this material.

4.1 *Relationship between ζ and z in softening–hardening material*

The relationship between ζ and z was defined by Valanis[17] as

$$\frac{d\zeta}{dz} = f(\zeta) \tag{41}$$

where $f(\zeta) > 0$. In the same paper, the linear form $f(\zeta) = 1 + \beta\zeta$ was chosen to describe the strain hardening materials in which β was a positive constant. To describe the strain softening behavior, it is now proposed that the linear form $f(\zeta) = 1 - \beta_s\zeta$ be used, so that

$$\frac{d\zeta}{dz} = 1 - \beta_s\zeta \quad (\beta_s > 0) \tag{42}$$

or

$$\zeta = \frac{1}{\beta_s}(1 - e^{-\beta_s z}) \tag{43}$$

where β_s is a material parameter.

For strain softening–hardening materials, a critical intrinsic time ζ_{cr} is introduced to indicate the point of change over from softening to hardening in a stress–strain curve. Thus, ζ_{cr} is also a material parameter. Equations (42) and (43) are valid only in the range of $\zeta \le \zeta_{cr}$ (or $z \le z_{cr}$). In addition, $d\zeta/dz$ in eqn (42) must be greater than zero, i.e. $\zeta_{cr} < 1/\beta_s$. For metallic materials, the critical strain always exists in the small strain range, so that the above constraint is automatically satisfied. For $\zeta > \zeta_{cr}$, where the material behavior is hardening, another form of $f(\zeta)$ is proposed. It reads

$$\frac{d\zeta}{dz} = b_h\, e^{\beta_h(z - z_{cr})}, \quad z \ge z_{cr} \tag{44}$$†

or

$$\zeta = \zeta_{cr} - \frac{b_h}{\beta_h}[1 - e^{\beta_h(z - z_{cr})}], \quad z \ge z_{cr} \tag{45}$$

where b_h and β_h are material parameters associated with the strain hardening part. Thus the relationship between ζ and z is shown in eqns (43) and (45) which validates the range before and after the critical point, respectively. If the ζ–z relation is assumed to be smooth, then it

†Equation (44) can be rewritten as

$$dz = \frac{d\zeta}{b_h + \beta_h(\zeta - \zeta_{cr})}$$

which for virgin state ($b_h = 1$, $\zeta_{cr} = 0$) reduces to eqn (41) with $f(\zeta) = 1 + \beta\zeta$.

should be differentiable at the critical point, and eqns (42) and (44) must be equal at ζ_{cr}. It follows that

$$b_h = e^{-\beta_s z_{cr}}. \tag{46}$$

Thus, b_h may be calculated if β_s and z_{cr} are known. The relation between ζ and z is plotted in Fig. 9. This curve shows that ζ is a smooth function of z in the whole range under the condition of eqn (46). In addition, the first derivative of the curve is continuous for the whole range. The second derivatives of the functions before and after the critical point can be found by differentiating eqns (42) and (44). They are found to be

$$\frac{d^2\zeta}{dz^2} = -\beta_s e^{-\beta_s z}, \quad z \le z_{cr} \tag{47}$$

and

$$\frac{d^2\zeta}{dz^2} = \beta_h b_h e^{\beta_h (z - z_{cr})}, \quad z \ge z_{cr} \tag{48}$$

Since the material parameters β_s, β_h and b_h are all positive, it may be observed from eqns (47) and (48) that the second derivative $d^2\zeta/dz^2$ is less than zero for softening and greater than zero for hardening behavior. The present definition for ζ–z relation is thus different from that by Valanis [24]. The latter defines that the first derivative $d\zeta/dz$ is greater than 1 for hardening and less than 1 for softening. In addition, the following explicit form was proposed in [24] for strain softening behavior

$$\frac{dz}{d\zeta} = 1 + \beta z, \quad (\beta > 0) \tag{49}$$

or

$$\zeta = \frac{1}{\beta} \log(1 + \beta z). \tag{50}$$

However, using this ζ–z relation, the constitutive equation could not be written in a closed form. On the other hand, the relationship for ζ–z defined by eqn (42) will lead to a constitutive equation in closed form. Comparison with the experimental results shows that the definition of [24] is not always correct in the behavior of strain softening–hardening materials. In Fig. 8, the

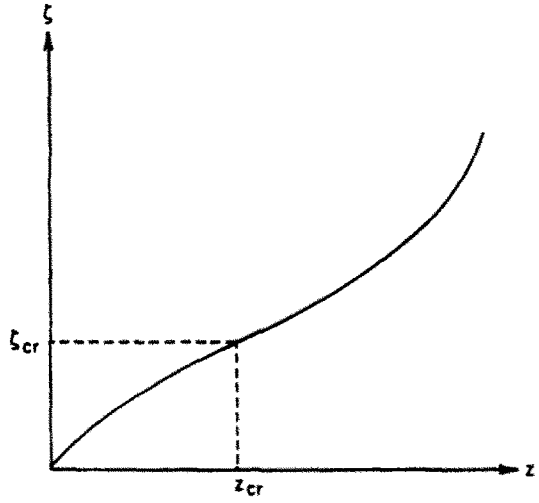

Fig. 9. Relationship between ζ and z for b.c.c. metallic materials.

strain softening behavior started at point A can be described by both definitions discussed above. However, the strain hardening occurred at point B can only be described by the definition given by eqns (47) and (48). According to the definition of Ref. [24], the strain hardening will occur at a point where the stress is higher than the stress at B, unless it is allowed to have a discontinuous $d\zeta/dz$ at ζ_{cr}. Using the z–ζ relations defined in eqns (47) and (48), the constitutive equation with strain rate and strain rate history effects of b.c.c. metallic materials can be obtained.

4.2. *Strain rate effect in the constitutive equation*

The constitutive equation for b.c.c. material is separated into the strain softening and the strain hardening parts. The strain softening part is first considered: this behavior occurs when $\zeta \leq \zeta_{cr}$. Since the strain rate sensitivity function k is assumed to be a constant for a specific strain rate, eqns (12), (15), (16) and (42) can be combined to give

$$\sigma = \frac{\sigma_y^0}{k}(1-\beta_s\zeta)\{1-(1-\beta_s\zeta)^{n_s^0+k_1/1-k_1}\}+\frac{\sigma_0^0-\sigma_y^0}{k}(1-\beta_s\zeta)\{1-(1-\beta_s\zeta)^{n_s}\}+\frac{E_2\zeta}{k} \tag{51}$$

where

$$\frac{\alpha}{\beta_s}-1=n_s \tag{52}$$

and

$$\frac{\alpha_0}{\beta_s}-1=n_s^0. \tag{53}$$

The material parameters obey the following relations:

$$\frac{E_0}{\beta_s(n_s^0+k_1)}=\sigma_y^0 \tag{54}$$

$$\frac{E_1}{\beta_s n_s}=\sigma_0^0-\sigma_y^0 \tag{55}$$

and

$$\beta_s=\frac{E_2-E_t^s}{\sigma_0^0} \tag{56}$$

where σ_y^0 is the yield stress of the reference stress–strain curve; E_t^s is the tangent modulus of the asymptotic straight line of the reference stress–strain curve in the softening part at large θ; and σ_0^0 is the intercept of this asymptotic line on the stress axis, as k_1 approaches 1. Equation (51) can be reduced further to the following equation for $0<\zeta\leq\zeta_{cr}$

$$\sigma=\frac{1-\beta_s\zeta}{k}[\sigma_0^0-(\sigma_0^0-\sigma_y^0)(1-\beta_s\zeta)^{n_s}]+\frac{E_2\zeta}{k} \tag{57}$$

and

$$\theta=\zeta/k. \tag{58}$$

Equation (57) is the constitutive equation for strain softening behavior of b.c.c. materials subjected to a prescribed strain rate.

As the strain increases, the material changes from softening into hardening at the critical

point ζ_{cr}. For $\zeta > \zeta_{cr}$ and $k_1 \to 1$, the following constitutive equation may be derived:

$$\sigma = \frac{b_h \sigma_0^0}{k}\left(1+\frac{\beta_h}{b_h}\bar{\zeta}\right)+\frac{\sigma_{0cr}^0-\sigma_{cr}^0}{k}\left(1+\frac{\beta_h}{b_h}\bar{\zeta}\right)\left[1-\left(1+\frac{\beta_h}{b_h}\bar{\zeta}\right)^{-n_h}\right]+\frac{E_2\zeta}{k} \tag{59}$$

and

$$\theta = \zeta/k \tag{60}$$

where

$$\frac{\alpha_0}{\beta_h}+1 = n_h^0 \tag{61}$$

$$\frac{\alpha}{\beta}+1 = n_h \tag{62}$$

$$\frac{b_h E_0}{\beta_h(n_h^0-k_1)} = b_h \sigma_y^0 \tag{63}$$

$$\frac{b_h E_1}{\beta_h n_h} = (\sigma_{0cr}^0-\sigma_{cr}^0)+b_h(\sigma_0^0-\sigma_y^0) \tag{64}$$

$$\frac{\beta_h}{b_h} = \frac{E_t^h-E_2}{\sigma_{0cr}^0-\sigma_{cr}^0+b_h\sigma_0^0} \tag{65}$$

and

$$\bar{\zeta} = \zeta - \zeta_{cr} \tag{66}$$

in which σ_{cr}^0 is the stress on the references stress–strain curve at the critical point; E_t^h is the tangent modulus of the asymptotic straight line at large strain; and σ_{0cr}^0 is the intercept of this asymptotic line of the reference curve with the vertical stress axis passing through $\theta = \theta_{cr}$. The material parameters mentioned above are shown in Fig. 10.

The stress–strain relation of softening–hardening material under constant strain rate for the ranges before and after the critical point is thus expressed respectively by eqns (57) and (59). All material parameters involved can be determined from a reference stress–strain curve using the method described in Section 3 for the strain hardening material. Since the strain rate sensitivity function k is equal to σ_y^0/σ_y (or σ_0^0/σ_0), where σ_y and σ_0 are functions of the strain rate, the function can be determined from the experimental data.

The theoretical predictions are now compared with experimental data obtained by Campbell and Marsh[6] for mild steel. Based on these experimental data, and assuming that k is equal to

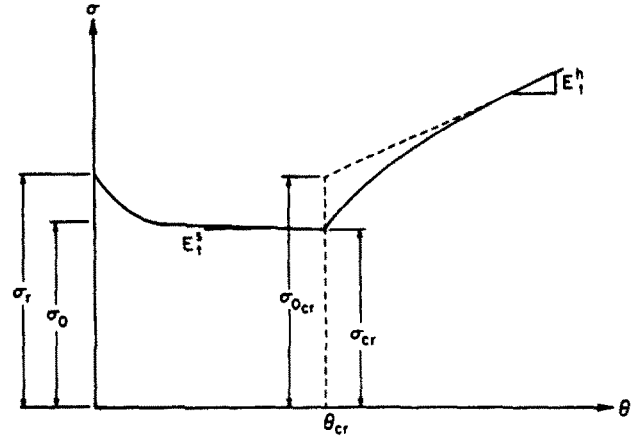

Fig. 10. Constant strain rate stress-plastic strain curve of b.c.c. metallic materials.

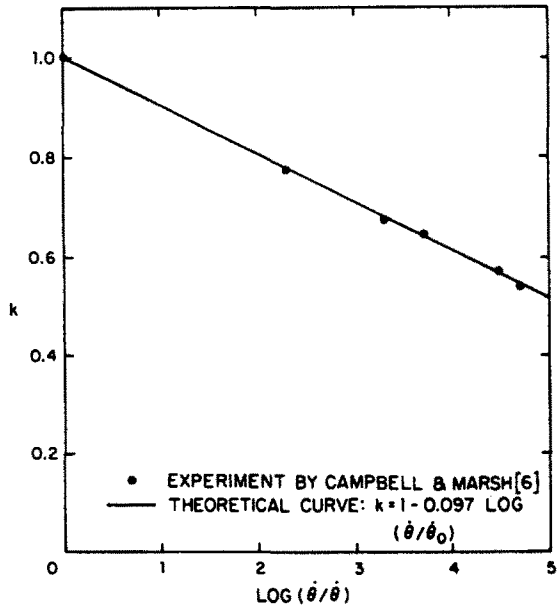

Fig. 11. The strain rate sensitivity function for mild steel.

1 on the reference stress–strain curve, Fig. 11 is constructed. It is seen that a logarithmic expression for k, as in the case of strain hardening materials, can fit the data nicely. In this calculation, the reference strain rate is taken as 10^{-4} per sec, and the following material parameters are used:

$$k = 1 - 0.097 \log_{10} \frac{\dot{\theta}}{\dot{\theta}_0}$$

$\sigma_y^0 = 35$ ksi $(2.41 \times 10^2$ MPa) $\quad \zeta_{cr} = 0.017$

$\sigma_0^0 = 29.5$ ksi $(2.03 \times 10^2$ MPa) $\quad n_s = 50$

$\sigma_{0cr}^0 = 35.5$ ksi $(2.45 \times 10^2$ MPa) $\quad n_h = 10$

$\sigma_{cr}^0 = 29.5$ ksi $(2.03 \times 10^2$ MPa)

$E_t^s = 0 \quad \beta_s = 8$

$E_t^h = 350$ ksi $(2.41 \times 10^3$ MPa) $\quad \beta_h/b_h = 3.654$

$E_2 = 236$ ksi $(1.63 \times 10^3$ MPa) $\quad b_h = 0.864.$

The results of the theoretical prediction and the experimental data for the dynamic stress–strain curves are shown in Fig. 12. The agreement in this figure is obviously good in the range of strain rate from 10^{-4} per sec to 5 per sec. It is seen that the critical strain increases with the strain rate.

4.3 *Strain rate history effect in the constitutive equation*

The strain rate history effect of strain hardening materials has been discussed in Section 3. A conclusion of the discussion is that the behavior of material varies with different history of strain rate. However, for a fixed strain rate history, a similar pattern of material behavior is obtained, independent of the strain magnitude at which the strain rate change takes place. The latter is no longer true for the strain softening–hardening materials. For this type of material, the subsequent material behavior is highly dependent on the strain magnitude at which the strain rate change occurs. The constitutive equations for strain rate change occurred before or after ζ_{cr} in both high–low and low–high test sequences can be obtained by use of eqns (42) and (44) in their valid range. Some calculated results are shown in Figs. 13–16 which will be further explained.

In 1961, Smith[10] presented experimental results of mild steel for both low–high and high–low strain rate change sequences in the case of $\zeta^* < \zeta_{cr}$. Figures 13 and 14 illustrate the

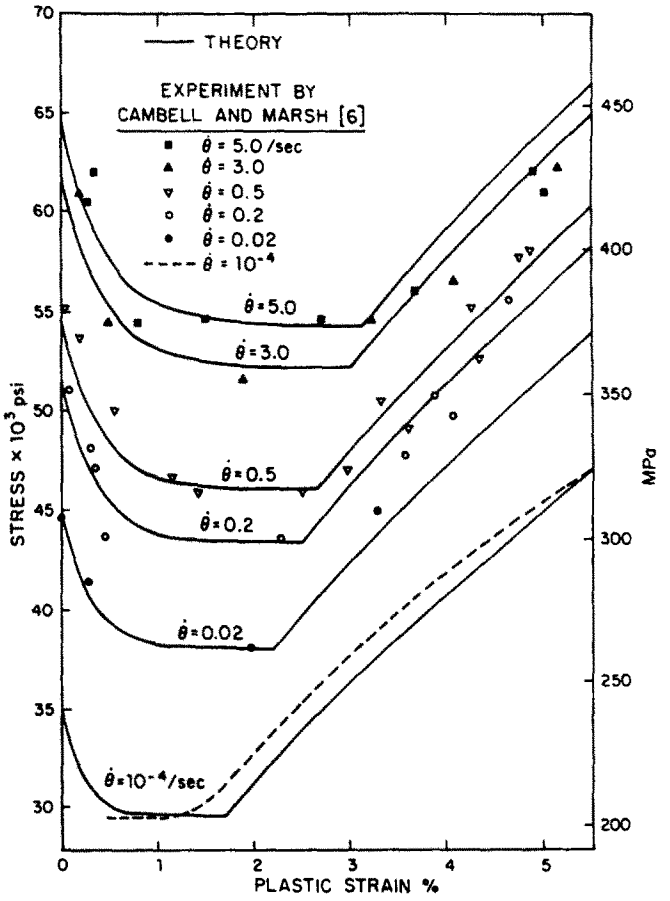

Fig. 12. Constant strain rate stress–strain curves for mild steel.

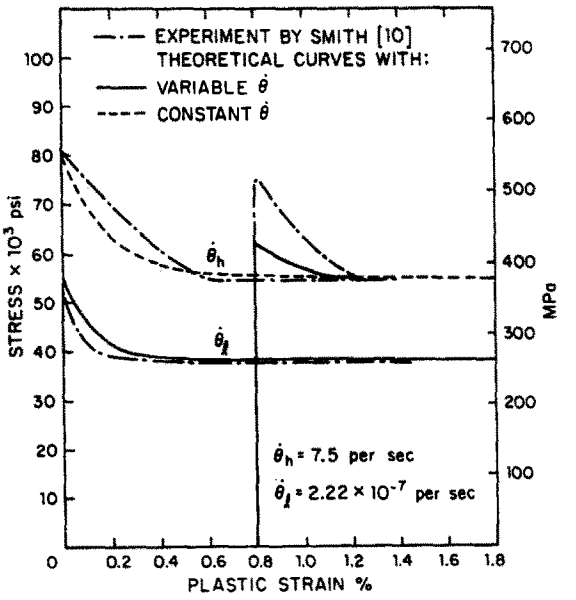

Fig. 13. Behavior of mild steel in tension under low–high strain rate change test sequence ($\zeta^* \leq \zeta_{cr}$).

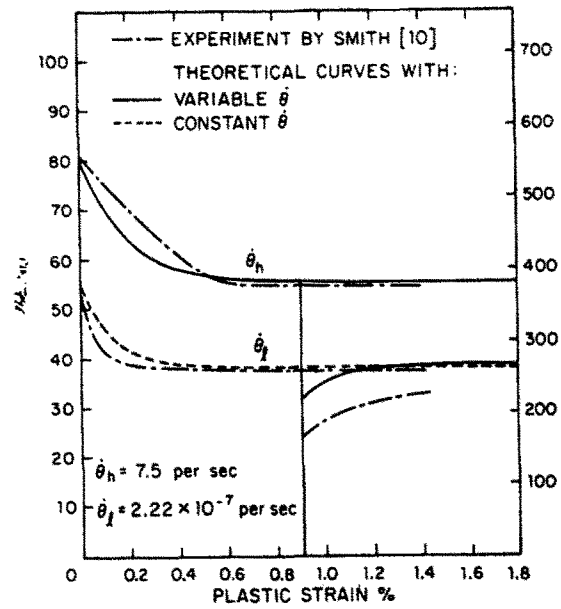

Fig. 14. Behavior of mild steel in tension under high–low strain rate change test sequence ($\zeta^* \leq \zeta_{cr}$).

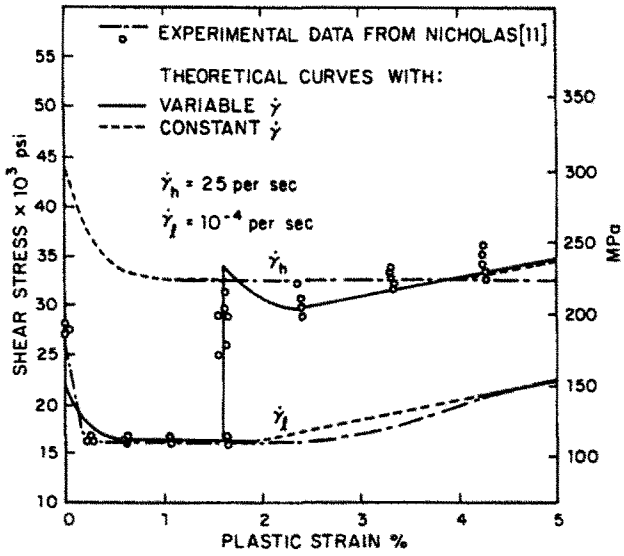

Fig. 15. Behavior of 1020 steel in shear under low–high strain rate change test sequence ($\zeta^* \leq \zeta_{cr}$).

theoretical curves together with the experimental data. In this calculation, the material parameters are determined as:

$$\sigma_y^0 = 55 \text{ ksi } (3.79 \times 10^3 \text{ MPa}) \qquad \beta_s = 5$$
$$\sigma_0^0 = 38 \text{ ksi } (2.62 \times 10^2 \text{ MPa}) \qquad n = 150$$
$$E_2 = 190 \text{ ksi } (1.31 \times 10^3 \text{ MPa}) \qquad k_h = 0.691$$
$$E_t^s = 0$$

and θ^* is equal to 0.8% in Fig. 13 and equal to 0.9% in Fig. 14. The strain rates for these two curves are 2.22×10^{-7} per sec and 25 per sec. The dotted lines in Figs. 13 and 14 denote the theoretical stress–strain curves at constant strain rate of 5 per sec and 2.22×10^{-7} per sec, respectively.

The strain rate history effect is not discussed in terms of the material response for b.c.c. and f.c.c. metallic materials. Figures 5 and 13 show the responses of stress and strain subjected to a

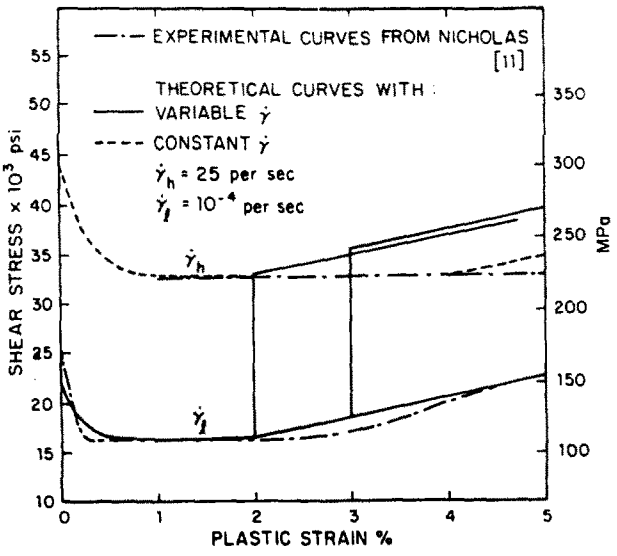

Fig. 16. Behavior of 1020 steel in shear under low–high strain rate change test sequence ($\zeta^* \geq \zeta_{cr}$).

change in strain rate from low to high for the two different kinds of material under investigation. It is seen that the responses are quite different. In Fig. 5, the strain rate varied curve is lower than the constant high strain rate curve after the change of strain rate. But this phenomenon is completely reversed in Fig. 13. The figure shows that after the change of strain rate, the strain rate varied curve overshoots the constant high strain rate curve. Moreover, both theory and experiment show an upper yield point immediately after the strain rate change. Whereas the theory did not predict an upper yield in Fig. 5, the experiment in this regard was inconclusive. A comparison of Figs. 7 and 14 also indicates a drastic difference in material response for high–low strain rate change sequence for the two types of material. For aluminum, the strain rate varied curve stays above the constant low strain rate curve and for mild steel, the static reloading curve is below the constant strain rate static curve (dotted line in Fig. 14). No upper yield point was indicated by both the theory and the experiment for mild steel. It is remarkable that the theory predicts qualitatively all the features of the material response under the above mentioned strain rate histories for both f.c.c. and b.c.c. metallic materials.

In 1971, Nicholas[11] also presented experimental curves to show the strain rate history effect of 1020 steel with a change in shear strain rate from 10^{-4} per sec to 25 per sec. Figure 15 shows the theoretical results and the experimental data. The material parameters used are:

$$\tau_y^0 = 22\ \text{ksi}\ (1.52 \times 10^2\ \text{MPa}) \qquad \beta_s = 12$$
$$\tau_0^0 = 16.25\ \text{ksi}\ (1.12 \times 10^2\ \text{MPa}) \qquad n_s = 50$$
$$E_2 = 195\ \text{ksi}\ (1.34 \times 10^3\ \text{MPa}) \qquad b_h = 0.76$$
$$\zeta_{cr} = 0.02 \qquad n_h = 10$$
$$\tau_{cr}^0 = 16.25\ \text{ksi}\ (1.12 \times 10^2\ \text{MPa}) \qquad \beta_h/b_h = 0.397$$
$$\tau_{0cr}^0 = 16.5\ \text{ksi}\ (1.14 \times 10^2\ \text{MPa})$$

In Fig. 15, the dash-dot-dash lines are experimental curves at high and low constant strain rates. The open circles are the data representing material response when the shear strain rate is changed from $10^{-4}/s$ to $25/s$ at $\theta = 1.6\%$.† It is seen from the figure that the varied strain rate curve is in qualitative agreement with the experimental data. The only possible discrepancy is that there exists an upper yield point in the theoretical curve immediately after the change of strain rate; whereas in the experimental data such an upper yield point is not apparent. Indeed, Nicholas[11] pointed out that there was no upper yield point in his experiment as opposed to

†It is assumed that $\zeta^* \leq \zeta_{cr}$ in this calculation. The case of $\zeta^* \geq \zeta_{cr}$ is discussed later in the text.

Smith's observation[10] which clearly indicated an upper yield point after a sudden increase in the strain rate.

No explanations were given by Nicholas or other researchers on the above mentioned observed discrepancy. It appears that the present theory can provide a consistent view on these seemingly incompatible observations. According to this theory, the above "discrepancy" is actually the expected results of mild steel when the change of strain rate takes place at different strain levels. Figure 16 shows the theoretical results for ζ^* equal to 0.02 and 0.03 which are greater than ζ_{cr}. Unfortunately, these curves cannot be compared with experimental results, since to the author's knowledge experimental results for $\zeta^* \geq \zeta_{cr}$ have not been reported in the literature. The material parameters used in the calculation are same as for Fig. 15. It is obvious that the curves in Fig. 16 do not have an upper yield point. Therefore, it may be concluded that whether an upper yield point appears in the reloading curve or not depends on where the change of strain rate takes place. If the change of strain rate occurs in the strain softening part of the stress–strain curve, then there will be an upper yield point upon reloading at a higher strain rate. On the other hand, if the change of strain rate occurs in the strain hardening range, then no upper yield point is expected to occur.

REFERENCES

1. J. Hopkinson, Further experiments on the rupture of iron wire. *Proc. Manchester Literary and Phil. Sol.* **11**, 119 (1872).
2. J. F. Bell, The dynamic plasticity of metals at high strain rates: an experimental generalization. *ASME Winter Annual Meeting* (1965).
3. E. A. Ripperger, Dynamic plastic behavior of aluminum, copper and iron, *ASME Winter Annual Meeting* (1965).
4. L. E. Malvern, Experimental studies of strain-rate effects and plastic wave propagation in annealed aluminum. *ASME Winter Annual Meeting* (1965).
5. U. S. Lindholm and L. M. Yeakely, Dynamic deformation of single and polycrystalline aluminum. *J. Mech. Phys. Solids* **13**, 41–53 (1965).
6. J. D. Campbell and K. J. Marsh, The effect of strain-rate on the post-yield flow of mild steel. *J. Mech. Phys. Solids* **11**, 49–63 (1963).
7. V. V. Sokolovsky, The propagation of elastic viscoplastic wave in bars. *Prikadnaia Matematika Mekhanika* **12**, 261–280 (1948).
8. L. E. Malvern, The propagation of longitudinal waves of plastic deformation in a bar of material exhibiting a strain-rate effect. *J. Appl. Mech.* **18**, 203–208 (1951).
9. J. D. Campbell and J. Duby, The yield behaviour of mild steel in dynamic compression. *Proc. R. Soc. Lond. Series A* **236**, 24–40 (1956).
10. R. C. Smith, Studies of effect of dynamic preloads on mechanical properties of steel. *Exp. Mech.* **1**, 153–158 (1961).
11. T. Nicholas, Strain-rate and strain-rate history effect in several metals in torsion. *Exper. Mech.* **11**, 153–158 (1971).
12. U. S. Lindholm, Some experiments with the split Hopkinson pressure bar. *J. Mech. Phys. Solids* **12**, 317–335 (1964).
13. J. Klepaczko, Strain rate history effects for polycrystalline aluminum and theory of intersections. *J. Mech. Phys. Solids* **16**, 255–266 (1968).
14. R. A. Frantz and J. Duffy, The dynamic stress–strain behavior in torsion of 1100-0 aluminum subjected to a sharp increase in strain rate. *J. Appl. Mech.* **39**, 939–945 (1972).
15. J. Klepaczko, Strain rate incremental test of copper. *Tech. Rep.*, Division of Engineering, Brown University (1974).
16. J. Klepaczko, R. A. Frantz and J. Duffy, History effects in polycrystalline f.c.c. metals subjected to rapid changes in strain rate and temperature. *Rozprawy Inzynierskie, Eng. Trans.* **25**, 3–22 (1977).
17. K. C. Valanis, A theory of viscoplasticity without a yield surface, Part I: General theory, Part II: Application to mechanical behavior of metals. *Archiwun Mechaniki Stosowanej* **23**, 517–551 (1971).
18. K. C. Valanis, Fundamental consequences of a new intrinsic time measure-plasticity as a limit of the endochronic theory. *Tech. Rep.*, Division of Materials Engineering, The University of Iowa (1978).
19. C. H. Karnes and E. A. Ripperger, Strain-rate effect in cold worked high-purity aluminum. *J. Mechs. Phys. Solids* **14**, 75–88 (1966).
20. R. Papirno and G. Gerard, Dynamic stress–strain phenomena and plastic wave propagation in metals. *Trans. ASM* **53**, 381–406 (1961).
21. C. H. Lin and H. C. Wu, Strain-rate effect in the endochronic theory of viscoplasticity. *J. Appl. Mech.* **43**, 92–96 (1976).
22. F. E. Hauser, J. A. Simmons and J. E. Dorn, Strain rate effects in plastic wave propagation. *Response of Metals to High Velocity Deformation*, (Edited by Shewmon and Zackay). Interscience, New York (1961).
23. P. E. Senseny, J. Duffy and R. H. Hawley, Experiments on strain rate history and temperature effects during the plastic deformation of close packed metals. *J. Appl. Mech.* **45**, 60–66 (1978).
24. K. C. Valanis, Effect of prior deformation on cyclic response of metals. *J. Appl. Mech.* **41**, 441–447 (1974).

APPENDIX

To obtain a more general form of the intrinsic time measure which accounts for strain rate, it is assumed that a spectrum of r intrinsic times exists and each intrinsic time corresponds to an internal state variable. Thus, for each intrinsic time

$$d\zeta_i^2 = h_i(\theta)\, d\theta^2 + g_i(\theta)\, dt^2, \quad i = 1, 2, \ldots, r \tag{A1}$$

where h_i and g_i are functions of θ, and t is the real time. The foregoing equation can be written as

$$d\zeta_i = \pm[h_i(\theta) + g_i(\theta)/\dot{\theta}^2]^{1/2}\, d\theta, \quad i = 1, 2, \ldots, r. \tag{A2}$$

Introducing an average intrinsic time measure ζ such that

$$d\zeta = \Lambda(d\zeta_1, d\zeta_2, \ldots, d\zeta_r) \tag{A3}$$

then

$$d\zeta = \Lambda[\pm(h_1(\theta) + g_1(\theta)/\dot{\theta}^2)^{1/2}, \quad \pm(h_2(\theta) + g_2(\theta)/\dot{\theta}^2)^{1/2}, \ldots, \pm(h_r(\theta) + g_r(\theta)/\dot{\theta}^2)^{1/2}]\, d\theta \tag{A4}$$

or

$$d\zeta = \pm k(\theta, \dot{\theta})\, d\theta \tag{A5}$$

where k, the strain rate sensitivity function, is a function of θ and $\dot{\theta}$. For simplicity, it is assumed that k is a function of $\dot{\theta}$ only, i.e.

$$d\zeta = k(\dot{\theta})|d\theta|. \tag{A6}$$

This relation is the same as that proposed earlier by Lin and Wu[21]. The only difference is that the total strain is now replaced by the plastic strain.